Published in final edited form as:
J Biomed Mater Res A. 2014 February ; 102(2): . doi:10.1002/jbm.a.34700.

Investigating Surface Topology and Cyclic-RGD Peptide functionalization on Vascular Endothelialization

Colton McNichols[1], **Justin Wilkins**[3], **Atsu Kubota**[3], **Yan T. Shiu**[3,4,*], **Samir M. Aouadi**[2], and **Punit Kohli**[1,*]

[1]Department of Chemistry and Biochemistry, Southern Illinois University, Carbondale IL 62901

[2]Department of Physics, Southern Illinois University, Carbondale IL 62901

[3]Department of Bioengineering, University of Utah, Salt Lake City, UT

[4]Division of Nephrology & Hypertension, Department of Internal Medicine, University of Utah, Salt Lake City, UT

Abstract

The advantages of endothelialization of a stent surface in comparison with the bare metal and drug eluting stents used today include reduced late-stent restenosis and in-stent thrombosis. In this paper, we study the effect of surface topology and functionalization of tantalum (Ta) with cyclic-(arginine-glycine-aspartic acid-D-phenylalanine-lysine (cRGDfK)) on the attachment, spreading, and growth of vascular endothelial cells. Self-assembled nano-dimpling on Ta surfaces was performed using a one-step electropolishing technique. Next, cRGDfK was covalently bonded onto the surface using silane chemistry. Our results suggest that nano-texturing alone was sufficient to enhance cell spreading, but the combination of a nano-dimpled surfaces along with the cRGDfK peptide may produce a better endothelialization coating on the surface in terms of higher cell density, better cell spreading, and more cell-cell interactions, when compared to using cRGDfK peptide functionalization alone or nano-texturing alone. We believe that future research should look into how to implement both modifications (topographic and chemical modifications) to optimize the stent surface for endothelialization.

Keywords

Surface Topology; Nanoporous; Cyclic-RGD Peptide functionalization; Vascular Endothelialization; Cell Growth

Introduction

Cardiovascular stent insertion provides a convenient way to re-open the lumen of arteries that have become stenotic or occluded, resulting in insufficient delivery of oxygen and nutrients. Stent technology began development in 1986[1], and since then many improvements have been made to make stents safer after their placement in the body. The main objective of stenting is to place a biocompatible material in the arteries to keep their lumen open and consequently maintain blood flow at a physiologically safe rate. Although many vascular problems have been corrected by modern day stents, a few issues remain unresolved.[1–3] The major complications of intracoronary stent placement include thromboembolic events (blocking of a blood vessel's lumen by a clot) and neointimal hyperplasia (thickening of the

*pkohli@chem.siu.edu
*y.shiu@hsc.utah.edu

blood vessel wall) due to smooth muscle cell hyperproliferation, leading to in-stent restenosis. Restenosis refers to the situation in which stenosis occurs after a period of stenting; literally meaning “re”stenosis. When a foreign object is placed inside the body, an immune response takes place. In the case of stenting, the body reacts by stimulating an inflammation response within the wall of the artery at and near the stent, which is followed by excessive proliferation of smooth muscle cells. This causes the muscular wall of the artery to thicken and can result in the collapse of the stent. A recent development in 2002[1], which is still used today, involves the release of drugs such as sirolimus, paclitaxel, rapamycin, and other immunosuppresants to suppress the immune response and smooth muscle cell over-proliferation, thereby minimizing and/or delaying restenosis or possible thrombosis. The drawback to this method is that the drugs also prevent the proliferation of the desired cell type - endothelial cell (EC) - on the stent.

The anti-inflammatory/anti-proliferative medicines are typically placed in a polymer coating or eluted via porous structures on the surface of the stent.[1] This drug elution method works well until the medicine is completely eluted or concomitant anti-platelet therapy is prematurely discontinued. Studies have shown that even a year after insertion of drug eluting stents (DES), myocardial infarction (commonly known as heart attack) due to restenosis remains even if aspirin, or secondary anti-platelet therapy, is ceased.[5] This problem, known as “late stent thrombosis,” signifies the need to develop new types of stents that do not contain the adverse effects of anti-proliferative or any cytotoxic drugs.

At least three solutions to this problem have been proposed: biodegradable, cell seeded, and vascular EC-promoting stents. The first type of stent, however, does not remain within the body, and hence, it cannot provide a permanent support for the arterial wall. Premature or uneven breakdown of the stent within the artery has been shown to cause an increased inflammatory response.[1] The cell seeding method is hampered by the limited sources of endothelial cells or stem cells derived from generic endovascular cells. This method has been studied more recently[1], but has not yet made significant progress. On the other hand, the endothelium-promoting stent has shown promise within the past decade. The central role of the vascular endothelium in preventing thrombosis and neointimal hyperplasia has led to strategies for restenosis prevention that focus on enhancing endothelial recovery. Such non-cytotoxic approaches differ from the cytotoxic approaches that are used by drug-eluting stents currently on the market. However, these non-cytotoxic approaches are still at the investigational stage and their long-term outcome is unknown. There have been a few different methods used for promoting endothelial growth on the stent surface. They include changing the surface texture of the stent[5–14], and applying a layer of endothelial promoting agents such as poly-L-Lysine,[15] titanium oxide,[16] cyclic-RGD peptide,[17–19] stem-cells,[1] or fibronectin[15]. Particularly, Desai and Webster have each pioneered the use of nanostructures in stent, drug-delivery, cell-nanostructures interactions.[6–14] The most cost effective and efficient method should be selected and studied using *in vitro* methods to test for endothelialization along with *in vivo* applications to test biocompatibility once a model prototype is developed. Once safely in place, the stent should develop a confluent layer of vascular endothelium at the stent-luminal interphase, separating the stent material from the blood flowing within the artery. This native endothelium creates a homogenous environment within the vessel. The anti-thrombotic nature of the endothelium will prevent clotting that could be associated with platelet-bare metal interaction,[20] as well as prevent platelet activation and mitogen release that could lead to smooth muscle cell proliferation and intimal hyperplasia. Palmaz et al found that parallel microscopic grooves on a metallic surface enhanced the migration rate of ECs.[20] The rate of migration, alignment, and elongation of ECs was enhanced as a function of groove size. An arranged non-random nanoporous structure has also shown to produce endothelial growth *in vitro* rapidly with a natural appearance according to samples studied under scanning electron microscopes.[6–14]

Moreover, Brammer et al. compared the behavior of ECs on flat titanium and the nanostructured surface of titanium nanotubes.[11] They reported that ECs spread, function and adhere better on a nanostructured surface of titanium nanotubes than flat surfaces.[11] The use of cell-binding motifs such as RGD-containing peptides on the surfaces can further enhance the adhesion, growth, and spreading of ECs on the surfaces[17–19] and may help in reducing the chance of restenosis. This design combined with a layer of cRGD peptide is thought to induce rapid endothelialization while preventing a detrimental immune reaction.

In this paper we study nanoporous architecture[5–16] and cRGD motif peptide[17–19]. The rate of endothelialization can be enhanced through a number of factors including: increasing EC migration speed, enhancing EC proliferation, increasing EC adhesion to the stent, and spreading on the stent surface. We hypothesize that the use of cRGDfK-functionalized nanoporous (specifically, nano-dimpled) stents will enhance the life-time of stents along with reducing the risk of restenosis compared to current DES or bare metal stents (BMS). The use of lifelong anti-platelet treatment may also be unnecessary if total endothelial coverage on the surface of stents is accomplished with the natural anti-thrombogenic properties of native endothelial cells.

Stents are usually produced using stainless steel, Tantalum (Ta), nitinol, or some other inert material.[30] These materials are mechanically ductile and can be expanded by the inflation of balloons inside of a blocked artery. Ta has several advantages when compared to the other materials. For example, Ta is a biocompatible and inert metal with less thrombogenicity than titanium or stainless steel.[30] Because of its high electron density, it is also used as a marker for identification when placed in the body for stents made of less dense materials. Unlike stainless steel, Ta does not interfere with magnetic resonance imaging (MRI) studies. Due to these advantages, Ta has been extensively used for stent fabrication along with titanium (Ti). Further, Ta has approximately six hydroxyl groups/nm^2 on its surface.[32] These hydroxyl groups can be used for surface modification with well-known silane chemistry to increase the functionality of the stent surface.[33]

In this paper, we fabricated nano-dimpled Ta surfaces using a one-step anodization of Ta. The surfaces were then covalently-modified with a cyclic-RGDfK peptide. We studied the effects of nano-dimples and surface functionalization with RGD-containing cyclic peptide cell-adhesion motif on endothelialization of the surfaces. We found that early phase cell spreading and later stage proliferation of endothelial cells was higher for the combination of surface-functionalized nano-dimpled substrates as compared to no-dimple (i.e., plain) and unfunctionalized surfaces. The results of this study enhance our knowledge on the growth and spreading of cells on nanostructure materials. This study may find potential implications in many areas of research including surface chemistry, implantable devices, and tissue engineering.

Methods and Materials

Materials

All the solvents for surface treatment were purchased from Fisher Scientific and were used as received unless otherwise noted in the text. 3-(triethoxysilyl) propylsuccinic anhydride (TSPA) and cyclic-(arginine-glycine-aspartic acid-D-phenylalanine-lysine) (cRGDfK) were purchased from Peptides International and Gelest Inc., respectively. cRGDfK was chosen because it is a well-known cell binding motif.[17,24] The characterization of the nano-dimpled tantalum (Ta) was performed using scanning electron microscopy. The functionalized TSPA and cRGDfK nano-dimpled surfaces were characterized with infra-red (IR) and mass spectroscopy (MS). The chemical structures of TSPA and cRGDfK are shown in Scheme 1. For cell experiments, Alexa Fluor 488-conjugated phalloidin and Hoechst 33342

(trihydrochloride, trihydrate FluoPure Grade) were purchased from Molecular Probes/Invitrogen (Carlsbad, CA), and the mounting solution was obtained from Vector Labs (Burlingame, CA). All other chemical reagents, cell culture glassware, and cell culture reagents were purchased from Fisher Scientific (Pittsburgh, PA) and Cambrex (East Rutherford, NJ), respectively, unless otherwise mentioned.

Substrates used in the studies

Four types of substrates were used for our studies: Ta with two different topologies (no-dimple (plain) and nano-dimpled) with and without covalently bound cRGDfK peptides. Nano-dimples were created using an electropolishing method described previously (see below).[25–28,32] All the substrates used for cell studies had a total planar (non-porous) area in the range of 1 to 2 cm^2.

Synthesis of nano-dimpled substrates

Electrochemical treatment of many metals provides nanoporous metal oxides. For example, the anodic oxidation of aluminum, tantalum (Ta), titanium, and other metals have been reported.[25–32] Nano-dimples were created on Ta surfaces using electropolishing in a solution composed of 95–98% sulfuric acid and 48% hydrofluoric acid (HF) in a volumetric 9:1 ratio (Figure 1).[25–28,32] *Caution: HF is highly toxic and dangerous to humans and animals. HF should be used in a well-vented hood and all safety precautions must be taken when using HF.* As pointed by Kruse's group, Ta surface likely to possess native oxide layer on its surface which can be stripped with HF during electropolishing step. Thus, by controlling the rate of oxide dissolution and formation, an array of nano-dimple on the surface is formed.[26,32] The typical area of the Ta samples used for electropolishing in our studies was approximately 1 to 2 cm^2. The polishing solution was kept at room temperature for a few hours prior to performing these experiments. Ta substrates (anodes) were kept at approximately 1.5 cm away from the platinum wire (cathode). A potential of 15 V was applied between two electrodes for 15 minutes. This technique produced nano-sized Ta dimples on the surface with ~4 nm thick TaO_2 top layer.

SEM characterization

To avoid charging of the sample, nano-dimpled Ta samples were coated with a thin layer (approximately 10 nm thick) of gold-palladium for electron microscopic characterization. All the samples were analyzed either on FEI Quanta 450 or Hitachi S570 using a secondary electron detector. The pore diameter of the nano-dimples was (23 ± 4) nm.

Surface-functionalization of plain and nano-dimpled Ta substrates

The surface functionalization with cRGDfK was accomplished using a two-step method (Scheme 1). In the first step, the surfaces were activated with TSPA which provided anhydride functionality on the surface for immobilizing amine-terminated cRGDfK peptides. The surfaces were soaked in 10 mM TSPA solution in dry dichloromethane for 3 hours. The surfaces were then thoroughly washed with dry dichloromethane to wash off unreacted TSPA from the surfaces. Reflection-absorption infrared spectroscopy on TSPA modified substrates showed a peak in 1792 cm^{-1} region which corresponds to carbonyl groups in the five-member succinic-anhydride group of TSPA (Figure S1). As a controlled experiment to show that TSPA-amine reaction occurs on surfaces, a reaction of 4-amino pyrene with succinic anhydride tagged on quartz substrates provided bluish fluorescent surfaces after a thorough washing with dichloromethane. The fluorescence from pyrene suggested the presence of succinic anhydride on the surface and its reaction with amine group of pyrene. The anhydride-functionalized Ta surfaces were immersed in a 10 μM

amine-terminated cRGDfK peptides dissolved in PBS buffer solution for 6–12 hours. The surfaces were then washed thoroughly in PBS or Tris buffer solution (pH 7.4).

Infra-red (IR) spectroscopy analysis of the samples

External reflection FTIR spectra of the functionalized Ta substrates were measured with Nicolet Nexus 670 FTIR fitted with nitrogen cooled MCT-B detector and a Velma II variable-angle specular-reflectance accessory operating at a beam incidence angle of 80° with respect to surface normal. The samples were averaged at 1000 scans and 2 cm^{-1} resolution against a background of a bare Ta substrate. The spectrometer was purged continuously with dry nitrogen gas to minimize water vapor in the sample chamber.

Mass spectroscopy (MS) analysis

MS was performed on unfunctionalized nano-dimpled Ta, TSPA- and cRGDfK-functionalized Ta using a Bruker Daltonics Microflex Time-of-Flight Mass Spectrometer. A pulsed nitrogen laser (337 nm, 20 kHz repetition rate) was used to desorb/ionize the sample, and the resultant ions were observed in the positive ion mode. The mass spectrum represented a sum of 500 individual mass spectra. The ion signals were observed in the m/z range from 20 to 1000.

Routine cell culture

Bovine aortic endothelial cells (BAECs) were purchased from Cambrex Biosciences and cultured in tissue culture dishes in Dulbecco's modified eagle medium supplemented with 5% fetal bovine serum, 1% sodium pyruvate, and 1% penicillin streptomycin. This mixed solution was referred to as complete DMEM. BAECs were incubated in humidified 5% CO_2/95% air at 37°C in an incubator. When cells became confluent, they were removed from the petri dishes by Trypsin and then placed into new dishes. Only cells with low passage numbers were used for the present study.

Preparing Ta samples for seeding cells

Prior to seeding BAECs, the various Ta samples were cleaned and sterilized by the following protocol: they were rinsed with sterilized nanopure water, immersed in an 70% ethanol bath for 1 minute, rinsed with sterilized nanopure water, immersed in an 70% ethanol bath again but for 5 minutes, allowed to air dry, and exposed to UV for 15 minutes on both sides in a biosafety cabinet.

Seeding BAECs on Ta samples

Different Ta samples: (1) no-dimple (plain) Ta without peptides, 2) plain Ta with peptides, 3) nano-dimpled Ta without peptides, and 4) nano-dimpled Ta with peptides were placed into separate wells of a 12-well plate (Figure 2a). Each experiment had duplicates and $n \geq 3$. BAECs from the routine culture were removed from petri dishes using Trypsin and suspended in complete DMEM at approximately 100 cells/μL. 200 μL of BAECs solution was placed onto each sample (Figure 2b). The 12-well plate was rotated gently to distribute BAECs evenly for 45 minutes. 2 ml of complete DMEM was added to each well (Figure 2c) and the BAECs were incubated an additional 5.25 or 29.25 hours for a total of 6 and 30 hours, respectively, in humidified 5% CO_2/95 % air at 37°C in an incubator.

Fluorescent staining and microscopic imaging

Following the 6- or 30-hour incubation time, BAECs on each sample were washed three times with phosphate-buffered saline (PBS), fixed in 4% paraformaldehyde in PBS at room temperature for 15 minutes, and permeabilized in 0.2% Triton X-100 in PBS at room temperature for 15 minutes. The fixed and permeabilized cells were incubated in a solution

consist of 5 μg/ml Hoechst 33342 in distilled H_2O for 30 minutes to stain nuclei (the stained nuclei emit blue fluorescence). After incubation, cells were washed three times with PBS and incubated in Alexa Fluor 488-conjugated phalloidin diluted with PBS for 60 minutes to stain actin fibers (the stained actin fibers emit green fluorescence) (Figure 2d). Finally, the mounting solution was added and the stained cells were sealed with a coverslip glass. Fluorescent microscopic images of the cells were observed using a Hamamatsu ORCA-ER digital camera attached to an Olympus IX70 microscope. DAPI and FITC filters were used for the nuclei and actin filaments imaging, respectively. For determining cell density, four randomly selected areas were taken from each Ta sample using a 20X objective (lower magnification). A 40X objective (higher magnification) was used for determining cell spreading.

Microscopic image analysis and data presentation

To determine the cell density, the number of cells in each of the four randomly selected areas (specifically, the number of the stained blue nuclei in each field of view) of each sample was counted using ImageJ (a Java image processing program from NIH). Briefly, lower magnification images were imported into ImageJ and processed into binary format, rendering the blue nuclei as black particles. Next, the number of BAECs was counted for each image by using the black particle analysis command in ImageJ, and the cell density was reported as the number of BAECs per cm^2. The final cell density for each surface type was calculated by averaging results from three or more experiments. For cell spreading, the higher magnification images (Figure 4) were analyzed to assess quantitatively morphology of BAECs (specifically, area of the cells) using ImageJ. Briefly, the edge of each fluorescently labeled cell body (green color) was manually traced, and the enclosed area was then calculated in ImageJ. The calculated result was reported as the area (μm^2) per cell, and the final "area per cell" for each surface type was calculated by averaging results from three or more experiments. $n \geq 3$ for all experiments, and statistical analysis was performed using Student's *t* test.

Results and Discussion

Figure 3 shows a typical SEM of nano-dimpled surface prepared by anodic oxidation of Ta in HF/H_2SO_4 mixture. The dimples (i.e., pores) are hexagonal packed with a diameter of 23 ± 4 nm. Ta anodic oxidation treatment provides a pore depth ~8–10 nm in the film of which about 4 nm thick tantalum oxide is top-most layer.[26,32] The modification of nano-dimple Ta can provide surfaces with a wide variety of functionalities that are otherwise hard to obtain. We utilized the RGD-motif for the functionalization of nanoporous Ta using a two-step reaction (Scheme 1). First, the surface was activated by reacting Ta surface with TSPA. The anhydride species were then reacted with amine-terminated cRGDfK (Scheme 1). The reaction of anhydride with amine from the lysine groups present in the peptide provides highly stable amide bonds. Figures S1A and S1B show the IR spectra before and after immobilization of cRGDfK on a TSPA-functionalized surface. It is known that peaks in 1775–1870 cm^{-1} region in the IR spectrum is an indicative of asymmetric C=O stretching resonance in a cyclic anhydride which blue-shifts to lower frequency after opening of the ring.[33] A peak at 1792 cm^{-1} in our FTIR spectra is attributed to asymmetric C=O stretching of the succinic anhydride which completely disappeared after addition of cRGDfK peptide on the surface. The disappearance of carbonyl stretching peak of succinic anhydride suggests a reaction between the amine group of lysine in cRGDfK and succinic anhydride of the TSPA on the surface (Figure S1). Our mass spectroscopic analysis on a physisorbed cRGDfK on unfunctionalized-Ta surface showed a peak at 603.31 m/z (corresponding to cRGDfK) confirmed the presence of cRGDFK on these surfaces, but a lack of m/z corresponding to 603.31 confirmed covalently immobilization of cRGDfK on the TSPA-

functionalized surfaces. Furthermore, the peaks at 1674 cm^{-1} and 1565 cm^{-1} in the FTIR spectrum are attributed to amide I (C=O) and amide II (N-H) respectively reinforced the above argument regarding the formation of peptide bonds on the surface.

We next analyzed cell density and area of cells present on the modified surface. We selected these two functionality factors (cell density and cell area) because they are closely related to our intended applications: when a bare stent is placed in a patient, a rapid increase in its coverage by cells requires rapid cell attachment and spreading, as well as an increase in cell number over time. The BAEC adhesion and morphology vary depending on stent surface topography and existence of cRGDfK peptide coating on the surface. Figures 5 and 6 summarize the cell density and cell area, respectively, on the four types of Ta surfaces. The representative fluorescent images of BAECs on samples with different surface topography/cRGDfK are shown in Figure 7.

Effect of topology and surface functionalization on cell density

We first consider the cell density 6 and 30 hours after seeding (Figure 5). The cells need to attach to a surface, in order to spread and continue to survive, growth and proliferate. We found that, within 6 hours, cell density on the non-functionalized plain and nano-dimpled surfaces was comparable to each other, but was approximately two-fold higher than the cell density on the functionalized plain and nano-dimpled surfaces. Thus, during this short period, at the first glance, functionalization appeared to have a significant inhibitive effect on cell density, but the nanopatterning did not appear to affect cell density. Our results showed a negative relationship between cell density and functionalization during this short initial period, which was not what we had anticipated. A possible explanation is that more cells could attach to the non-functionalized surface through non-specific binding interactions, whereas cells could only attach to the functionalized surface through specific receptor-ligand binding interactions. Strong cell attachment and normal cell spreading onto the surface is mediated by the interactions between cell receptors and RGD-motif ligands on the surface. As mentioned above, the cells need to attach to and spread on the surface in order to survive, growth and proliferate. Thus, even though there were more cells on the non-functionalized surface within the short period of time, these cells may not attach to or spread well on the surface, and hence may not proliferate well. We found an approximately two-fold increase in the cell density on the functionalized surfaces (plain or non-dimpled) following 30 hours of incubation (Figure 5). On the other hand, under the same experimental conditions, the cell density on the non-functionalized surface (plain or nano-dimpled) dropped significantly from 6 hours to 30 hours (Figure 5). This suggests that while there were more cells on the non-functionalized surface within first 6 hours growth period, these cells may not have attached to the surface strongly, leading to lower cell spreading and proliferation as compared to functionalized surfaces. It is interesting to note that, after 30 hours of incubation on functionalized surfaces, the plain surface had more cells than the nano-dimpled surface (Figure 5). Thus, functionalization appeared to have a more positive effect on cell proliferation as compared to surface topography.

Effect of topology and surface functionalization on cell spreading

Within the first 6 hours, the average cell area seemed to be smaller on the plain surface than on the nano-dimpled surface (particularly without cRGDfK coating on the surface (Figure 4)). Although BAECs can spread out and develop actin filaments on all surfaces within 6 hours, they formed more defined lamellapodia (arrow heads in Figure 4) and filapodia (arrows in Figure 4) on the nano-dimpled than the plain surfaces that were not coated with cRGDfK. Though, such a trend (i.e., larger cell area on nano-dimpled surface than on plain surface) was not statistically significant, regardless of functionalization (Figure 6). After culture for 30 hours, the cell area increased with time on the nano-dimpled surface, whereas

the cell area seemed to remain unchanged on the plain surface, regardless of functionalization (Figure 6). Indeed, the cell area on the nano-dimpled surface after 30 hours of incubation was significantly larger than the cell area on the plain surface after 6 hours of incubation, regardless of functionalization (Figure 6). Thus, the surface topography appeared to have a more positive effect on the cell spreading when compared to surface functionalization. Our finding that surface patterning shows a tendency to enhance cell spreading is consistent with the literature where authors recently reported an enhanced keratinocyte spreading on nano-textured surfaces as compared to unmodified substrates.[7]

In summary, we found that, to achieve an increased cell density over time, functionalization appeared to have a more positive effect than surface topography (Figure 5). Surface topography also appeared to have a more positive effect than functionalization on increased cell area over time (Figure 6). Therefore, it is likely that the combined surface modification is optimal for promoting endothelialization and may have several advantages with regard to clinical applications. Our results suggested that nanopatterning enhances spreading during the initial phase; i.e., during the shorter (6 hours) growth period when cells come into contact with the surface. Quick cell spreading, and hence, increased coverage of the stent with endothelial cells can prevent or minimize the contact between platelets and the stent. Our results also suggest that peptide functionalization exhibited an advantageous effect on increase in cell density after 30 hours of growth time. Therefore, future research should look into how to implement both modifications (topographic and chemical modifications) to optimize the stent surface for endothelialization. Finally, it is worth mentioning that a longer growth time for nano-dimpled and functionalized surfaces resulted in cell-to-cell interactions (arrows in Figure 7). We did not perform rigorous analysis of cell-cell junction formation, which is worthy of exploration in the future.

Our results suggest that a combined topography and functionalization modifications may lead to an enhanced spreading of cells on the stent surfaces, and eventually can create a confluent layer with intact cell-cell junctions through cell growth and spreading. The uniform coverage of the stent surface will be highly beneficial because it will reduce the growth of smooth muscle cells and adsorption of other biological materials on stents, thus, reducing the probability of late-stent restenosis and in-stent thrombosis. Further, funtionalized-nanodimple coating may find applications in other implantable devices where uniform coating with reduced defects may help in reducing infection and inflammation due to non-specific biomolecular adsorption on the devices.

Conclusion

We fabricated nano-dimpled Ta surfaces using a simple one step electropolishing step. We covalently tagged the nano-dimpled surface with cRGDfK peptide. We observed that topographic and chemical modifications had different but important roles in promoting endothelialization. (1) Nanopatterning enhanced cell spreading (larger cell area) at both the early and late phases of the cell growth. (2) Functionalization appeared to enhance the cell proliferation (larger cell density) at the later phase. (3) Finally, it seemed that by combining nano-texturing and cRGDfK peptide functionalization, better cell-cell junctions may be achieved than nano-texturing or functionalization alone.

Supplementary Material

Refer to Web version on PubMed Central for supplementary material.

Acknowledgments

We acknowledge the National Institutes of Health for partial financial support (NIH to PK and SA) and the National Science Foundation (CAREER award to PK). YTS is supported by grants from the National Institutes of Health (R01HL67646 and R01DK088777). We thank Dr. Peter Kruse for help in the fabrication of the electropolished nano-dimpled Ta. Brandon Luster's assistance in the acquisition of SEM images is also acknowledged. We thank D'Arcy Stone for her advice in producing metal surfaces. An FE-SEM instrument (FEI Quanta 450) was purchased through a grant from NSF (GM 8071101) is greatly acknowledged. We thank Dr. Laura M. Chapin for critically reading the manuscript.

References

1. Smith, Elliot J.; Jain, Ajay K.; Rothman Martin, T. New Developments in Coronary Stent Technology. Journal of Interventional Cardiology. 2006; 19:493–99. [PubMed: 17107363]
2. Serry, Rod; Penny, William F. Endothelial Dysfunction After Sirolimus-Eluting Stent Placement. Journal of the American College of Cardiology. 2005; 46:237–238. [PubMed: 16022948]
3. Chatterjee, Subroto; Pandey, Ambarish. Drug Eluting Stents: Friend or Foe? A Review of Cellular Mechanisms Behind the Effects of Paclitaxel and Sirolimus Eluting Stents. Current Drug Metabolism. 2008; 9:554–566. [PubMed: 18680476]
4. McFadden, Eugene P.; Stabile, Eugenio; Cheneau, Edovard; Ong, Andrew T.; Kinnaird, Timothy; Suddath, William O.; Weissman, Neil J.; Torguson, Rebecca; Kent, Kenneth M.; Prichard, August D.; Satler, Lowell F.; Waksman, Ron; Serruys, Patrick W. Late thrombosis in drug-eluting coronary stents after discontinuation of antiplatelet therapy. The Lancet. 2004; 364:1519–521.
5. Nakayama, Yasuhide; Nishi, Shogo; Ishibashi-Ueda, Hatsue; Matsuda, Takehisa. Surface microarchitectural design in biomedical applications: In vivo analysis of tissue ingrowth in excimer laser-directed micropored scaffold for cardiovascular tissue engineering. Journal of Biomedical Materials Research. 2000; 51:520–28. [PubMed: 10880097]
6. Lu, Jing; Rao, Masaru P.; MacDonald, Noel C.; Khang, Dongwoo; WebsterThomas, J. Improved endothelial cell adhesion and proliferation on patterned titanium surfaces with rationally designed micrometer to nanometer features. Acta Biomaterialia. 2008; 4:192–201. [PubMed: 17851147]
7. Puckett SD, Lee PP, Ciombor DM, Aaron RK, Webster TJ. Nanotextured titanium surfaces for enhancing skin growth on transcutaneous osseointegrated devices. Acta Biomater. 2010; 6:2352–62. [PubMed: 20005310]
8. Khang, Dongwoo; Lu, Jing; Yao, Chang; Haberstroh, Karen M.; Webster; Thomas, J. The role of nanometer and sub-micron surface features on vascular and bone cell adhesion on titanium. Biomaterials. 2008; 29:970–983. [PubMed: 18096222]
9. Zile, Melanie A.; Puckett, Sabrina; Webster, Thomas J. Nanostructured titanium promotes keratinocyte density. Journal of Biomedical Materials Research Part A. 2011; 97A:59–65.
10. Peng L, Eltgroth ML, LaTempa TJ, Grimes CA, Desai TA. The effect of TiO_2 nanotubes on endothelial function and smooth muscle proliferation. Biomaterials. 2009; 30:1268–1272. [PubMed: 19081625]
11. Ainslie KM, Tao SL, Popat KC, Daniels H, Hardev V, Grimes CA, Desai TA. In vitro inflammatory response of nanostructured titania, silicon oxide, and polycaprolactone. Journal of Biomedical Materials Research. 2008; Part A:647–655.
12. Brammer KS, Oh S, Gallagher JO, Jin S. Enhanced Cellular Mobility Guided by TiO_2 Nanotube Surfaces. Nano Letters. 2008; 8:786–793. [PubMed: 18251515]
13. Peng L, Barczak AJ, Barbeau RA, Xiao Y, LaTempa TJ, Grimes CA, Desai TA. Whole genome expression analysis reveals differential effects of TiO2 nanotubes on vascular cells. Nano Letters. 2010; 10:143–148. [PubMed: 20030358]
14. Peng L, Mendelsohn AD, Latempa TJ, Yoriya S, Grimes CA, Desai TA. Long-Term Small Molecule and Protein Elution from TiO_2 Nanotubes. Nano Letters <>9. 2009:1932–1936.
15. Wang GX, Deng XY, Tang CJ, Liu LS, Xiao L, Xiang LH, Quan XJ, Legrand AP, Guidoin R. The Adhesive Properties of Endothelial Cells on Endovascular Stent Coated by Substrates of Poly-L-Lysine and Fibronectin. Artificial Cells, Blood Substitutes, and Immobilization Biotechnology. 2006; 34:11–25.

16. Chai F, Ochsenbein A, Traisnel M, Busch R, Breme J, Hildebrand HF. Improving endothelial cell adhesion and proliferation on titanium by sol-gel derived oxide coating. Journal of Biomedical Materials Research Part A. 2010; 92:754–765. [PubMed: 19274713]

17. (a) Pierschbacher MD, Ruoslahti E. The cell attachment activity of fibronectin can be duplicated by small fragments of the molecule. Nature. 1984; 309:30–33. [PubMed: 6325925] (b) Ruoslahti E. RGD and other recognition sequences for integrins. Annual Review of Cell and Developmental Biology. 1996; 12:697–715.

18. Xiao, Yao; Truskey, George A. Effect of Receptor-Ligand Affinity on the Strength of Endothelial Cell Adhesion. Biophysical Journal. 1996; 71:2869–2884. [PubMed: 8913624]

19. Palmaz JC, Benson A, Sprague EA. Influence of Surface Topography on Endothelialization of Intravascular Metallic Material. Journal of Vascular and Interventional Radiology. 1999; 10:439–444. [PubMed: 10229473]

20. Pierschbacher MD, Ruoslahti E. Proceedings of the National Academy of Sciences of the United States of America. 1984; 81:5985–5988. [PubMed: 6237366]

21. Singh, Sherdeep; Festin, Miguel; Barden, Warren RR.; Xi, Luan; Francis, James T.; Kruse, Peter. Universal Method for the Fabrication of Detachable Ultrathin Films of Several Transition Metal Oxides. ACS Nano. 2008; 2:2363–2373. [PubMed: 19206404]

22. Singh, Sherdeep; Barden, Warren RT.; Kruse, Peter. Nanopatterning of Transition Metal Surfaces via Electrochemical Dimple Array Formation. ACS Nano. 2008; 2:2453–2464. [PubMed: 19206279]

23. Cai QY, Paulose M, Varghese OK, Grimes CA. The Effect of Electrolyte Composition on the Fabrication of Self-Organized Titanium Oxide Nanotube Arrays by Anodic Oxidation. Journal Materials Research. 2005; 20:230–236.

24. Martin CR. Nanomaterials: A Membrane-Based Synthetic Approach. Science. 1994; 266:1961–1966. [PubMed: 17836514]

25. Masuda H, Fukuda K. Ordered Metal Nanohole Arrays Made by a Two-Step Replication of Honeycomb Structures of Anodic Alumina. Science. 1995; 268:1466. [PubMed: 17843666]

26. Martin CR, Kohli P. The Emerging Field of Nanotube Biotechnology. Nature Drug Discovery. 2003; 29:2.

27. Zakeri, Rashid; Clay, Watts; Wang, Haibo; Kohli, Punit. Synthesis and Characterization of Non-linear Nanopores in Alumina Films. Chemistry of Materials. 2007; 19:1954–1963.

28. El-Sayed, Hany; Singh, Sherdeep; Greiner, Mark T.; Kruse, Peter. Formation of Highly Ordered Arrays of Dimples on Tantalum at the Nanoscale. Nano Letters. 2006; 6:2995–2999. [PubMed: 17163747]

31. Adam; Andreas; Dondelinger; Robert, F.; Mueller; Peter, R. Textbook of metallic stents. ISIS Medical media; 1997. p. 213

32. McCaerty E, Wightman JP. Determination of the Concentration of Surface Hydroxyl Groups on Metal Oxide Films by a Quantitative XPS Method. Surface Interface Analysis. 1998; 26:549–564.

33. Aubry D, Volcke C, Arnould Ch, Humbert C, Thiry PA, Delhalle J, Mekhalif Z. Molecular functionalization of tantalum oxide surface towards development of apatite growth. Applied Surface Science. 2009; 255:4765–4772.

34. Smith, B. Infrared Spectral Interpretation: A Systematic Approach. CRC Press; Boca Raton: 1998. p. 108

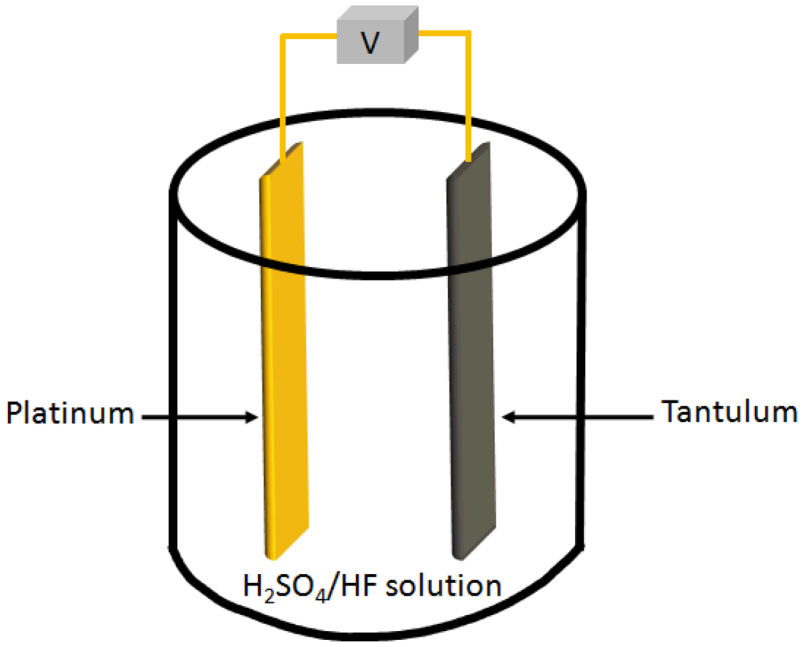

Figure 1.
Schematic diagram of the setup for the fabrication of nano-dimpled tantalum using electropolishing in a H_2SO_4/HF mixture.

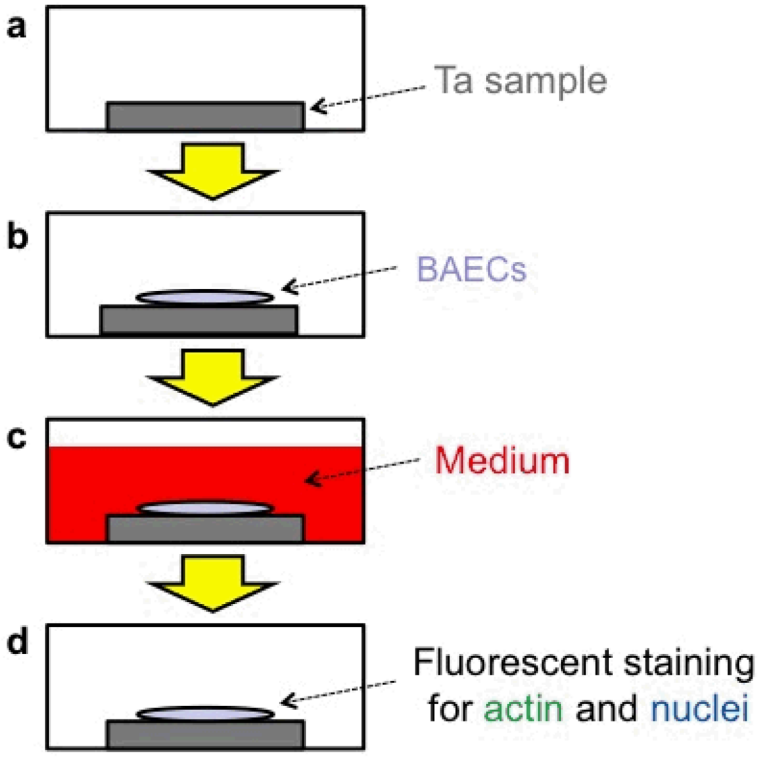

Figure 2.
Schematic of cell culture experiments. (a) A Ta sample was placed in one well of a 12-well plate. (b) 200 μL of bovine aortic endothelial cells (BAECs) at 100 cells/μL were placed on top of the sample and incubated for 45 minutes. (c) 2 ml of cell culture medium was added and the cells were incubated for a total of 6 or 30 hours. (d) The actin and nuclei were stained green and blue, respectively.

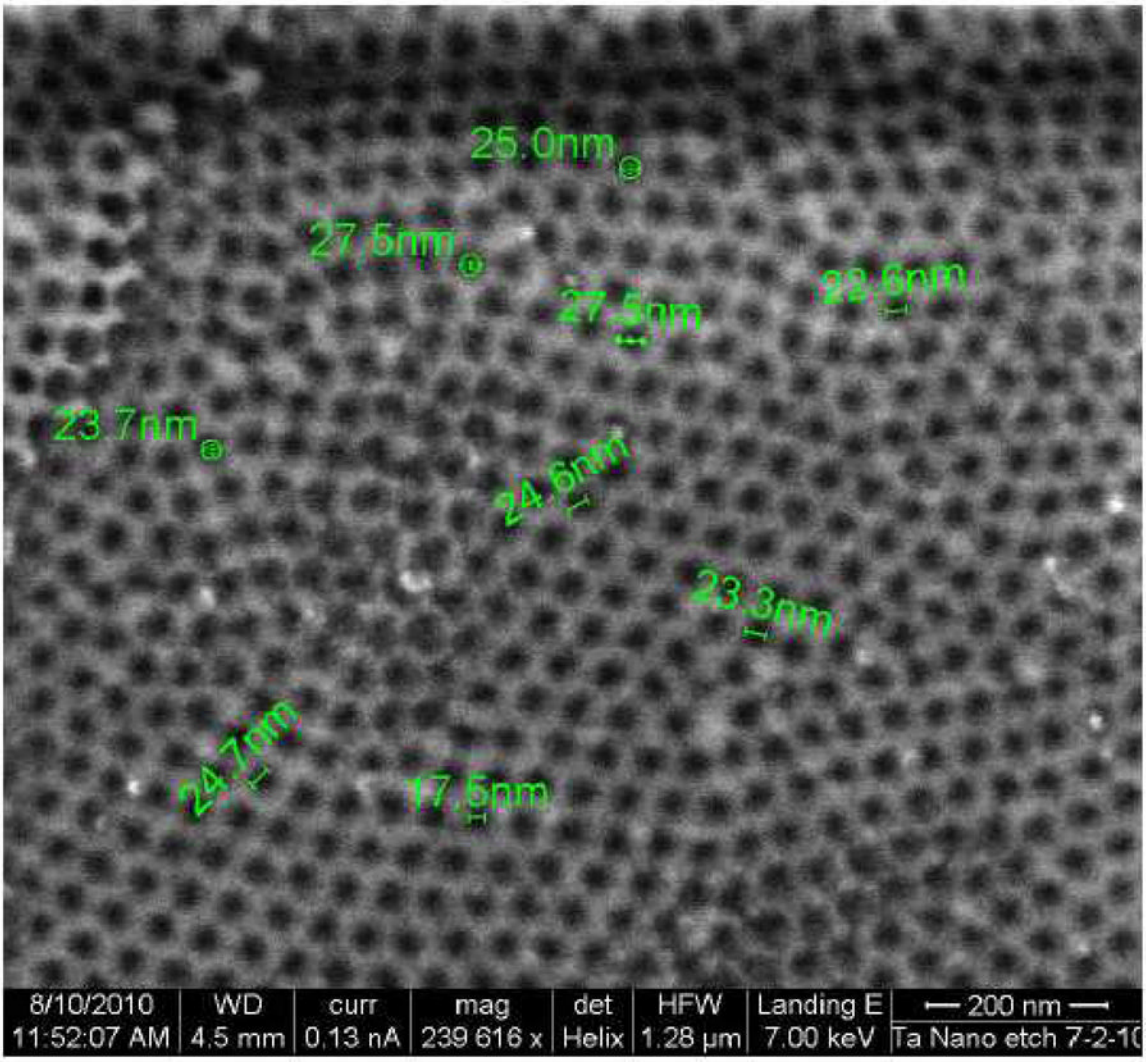

Figure 3.
A typical scanning electron micrograph of nano-dimpled Ta surface. The pore diameter is approximately 23 ± 4 nm.

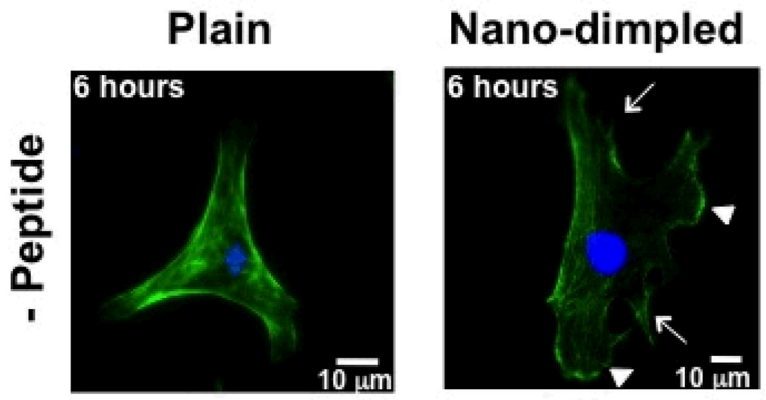

Figure 4.
Representative fluorescence optical micrographs of BAECs after culture for 6 hours on non-functionalized surfaces (40X objective). During this initial phase, although BAECs can spread out and develop actin filaments on both surfaces, they formed more defined lamellapodia (arrow heads) and filapodia (arrows) on the nano-dimpled than the plain tantalum surfaces.

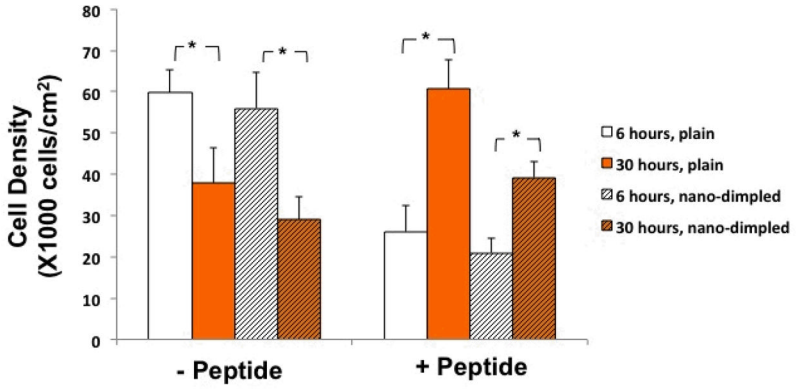

Figure 5.
Cell density on different substrates after culture for 6 and 30 hours.

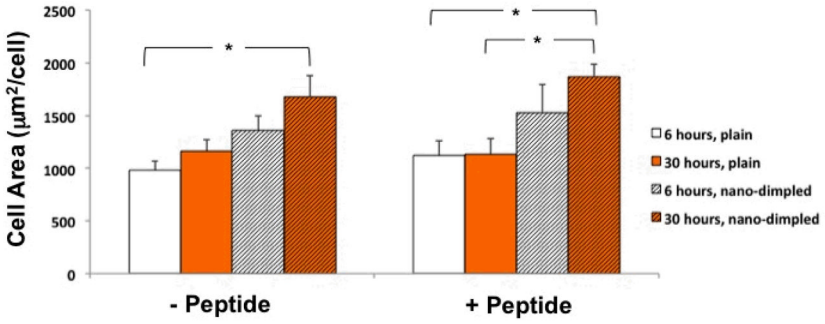

Figure 6.
Cell area on different substrates after culture for 6 and 30 hours.

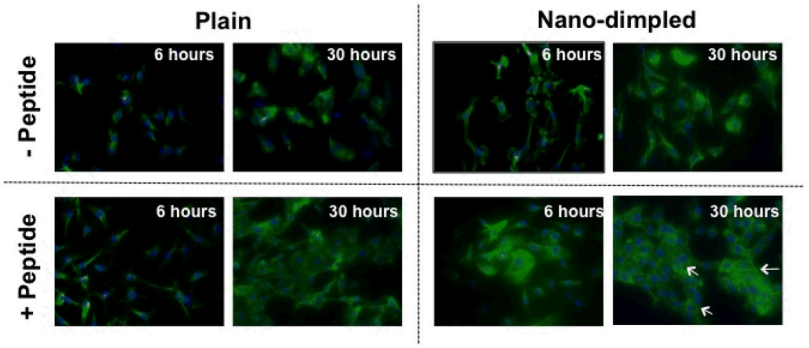

Figure 7.
Representative fluorescence optical micrographs of BAECs after culture for 6 and 30 hours (40X objective). Arrows point to cell-cell borders showing intense actin staining.

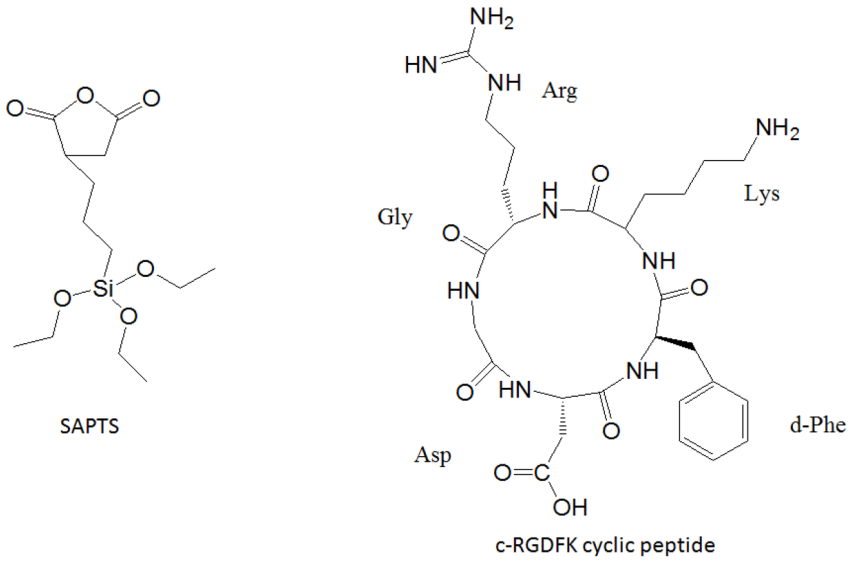

Scheme 1.
Chemical structures of TSPA and cRGDfK used in our studies.

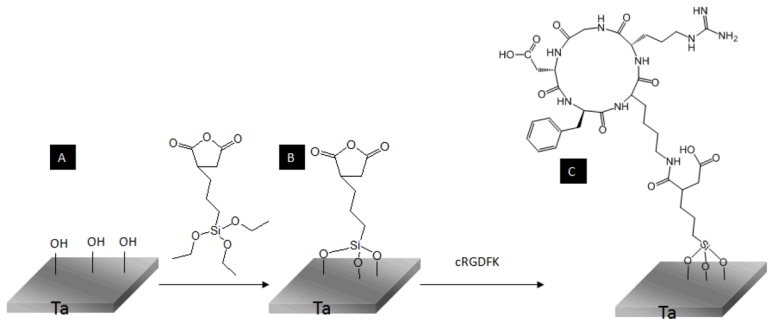

Scheme 2.
Schematic of the covalent immobilization of cRGDfK on the nano-dimpled Ta substrates using a two-step process.